Received: 8 January 2025 | Revised: 20 February 2025 | Accepted: 23 February 2025

DOI: 10.1002/jccs.202500009

JCCS JOURNAL OF THE CHINESE CHEMICAL SOCIETY

RESEARCH ARTICLE

Improved hydrogen evolution efficiency in water splitting with WO_3 thin film via physical vapor deposition

Muhammad Junaid[1] | **Mohamed Sharaf**[2] | **Mohammad El-Meligy**[3,4] | **Muhammad Amjad Riaz**[5] | **Mohd Arif Dar**[6] | **Irfan Ullah Khan**[7]

[1]Institute of Physics, The Islamia University of Bahawalpur, Bahawalpur, Pakistan

[2]Department of Industrial Engineering, College of Engineering, King Saud University Riyadh, Riyadh, Saudi Arabia

[3]Jadara University Research Center, Jadara University, Irbid, Jordan

[4]Applied Science Research Center, Applied Science Private University, Amman, Jordan

[5]Department of Chemistry, University of Education Lahore, Vehari Campus, Vehari, Pakistan

[6]Faculty of Allied Health Sciences, Chettinad Hospital, and Research Institute, Chettinad Academy of Research and Education, Tamil Nadu, India

[7]Department of Integrative Biology, The College of Arts and Sciences, Oklahoma State University, Stillwater, Oklahoma, USA

Correspondence
Muhammad Junaid, Institute of Physics, The Islamia University of Bahawalpur, 63100 Bahawalpur, Pakistan.
Email: mjunaid310@yahoo.com

Funding information
King Saud University, Grant/Award Number: RSPD2025R704

Abstract

WO_3 has successfully been deposited on indium tin oxide (ITO) substrate via physical vapor deposition (PVD) technique, and X-rays diffraction (XRD) confirmed the deposition of a thin layer that is orthorhombic. The XRD and linear sweep voltammetry (LSV) study of the WO_3 thin film confirmed the type of semiconductor and observed it to be an n-type semiconductor. The scanning electron microscopy (SEM) study revealed the uniform and porous morphology of the thin film, and the particle size of WO_3 was measured to be 34 nm without annealing. Fourier transform infrared (FTIR) confirmed the functional group and particle vibration (stretching, compression) the broad band of stretching of WO_3 is monoclinic and observed to be in the range of 3200–3500 cm^{-1}. The W-O-W peak is noted in the range of 400–500 cm^{-1}, while the W-O peak is recorded in the range of 700–900 cm^{-1}, and furthermore, minor peaks were also recorded in the range of 1400–1700 cm^{-1}. UV spectroscopy provided the absorbance of the solar spectrum in the UV and visible range beyond 400-nm range of wavelength. The maximum absorbance was noted in the UV range (320 nm) and gradually decreases with the wavelength. The maximum percentage transmittance was noted at a wavelength in the 500-nm range, which is 88.67%. The band gap of the deposited thin film was also confirmed via the Tauc plot and observed to be 3.26 eV. The Electrochemical impedance spectroscopy (EIS) small curve of WO_3 is evidence of the low impedance and large photocurrent. The maximum photocurrent confirmed from LSV measurement was noted to be 0.51% at 0.8 V, which is quite good for water-splitting applications. The hydrogen generation of the thin film through photoelectrochemical (PEC) water splitting was observed and found to have an average rate of 1743.09 mol g^{-1} for 6 h.

KEYWORDS

CO_2 reduction, green hydrogen, photocatalysis, solar water splitting

1 | INTRODUCTION

Green energy and sustainable development are closely related concepts, as green energy is an essential component of sustainable development. Green energy is regarded as energy that is generated from environmentally friendly renewable resources like solar, wind, hydro, geothermal, and biomass. Contrarily, sustainable development refers to growth that satisfies present needs without endangering the ability of future generations to meet their own needs [1]. It is a holistic approach to development that takes into account environmental, social, and economic factors and seeks to achieve a balance between them. The use of green energy is critical for achieving sustainable development because it reduces greenhouse gas emissions and other forms of pollution, preserves natural resources, and supports economic growth [2].

Thin films utilized in photocatalytic water splitting present several distinct benefits. Their high surface-area-to-volume ratio significantly enhances reaction efficiency by maximizing exposure to both light and reactants, which increases the number of active sites available for the reaction. Additionally, the compact structure of thin films facilitates efficient electron transport, reducing charge recombination, which in turn improves the overall photocatalytic performance. Thin films are also versatile, making them easily integrated into various devices, which hold potential for large-scale applications. Despite these advantages, there are challenges associated with thin films. The relatively small thickness of these films can limit light absorption, especially in materials that need deeper penetration of light for optimal catalytic action. Furthermore, producing high-quality thin films that maintain uniformity across their surface can be technically demanding and economically expensive. Another concern is the long-term stability of thin films, as they are susceptible to degradation under the rigorous conditions encountered during photocatalytic processes. In conclusion, while thin films offer considerable promise for water-splitting technologies, addressing their limitations related to light absorption, cost, and durability is crucial for making them viable for widespread use in sustainable energy applications [2–5].

WO_3 nanoparticles are tiny particles of the compound tungsten oxide, which is a wide bandgap semiconductor material. Tungsten oxide nanoparticles are of interest in the fields of nanotechnology and energy due to their unique electronic and optical properties, which make them suitable for use in a variety of applications, including gas sensing and energy conversion [6]. By altering their electrical resistance in response to the presence of the gas, tungsten oxide nanoparticles are used in gas sensing to detect a variety of gases, including carbon monoxide and nitrogen oxides. Compared to other types of gas sensors, this makes tungsten oxide-based gas sensors extremely sensitive and selective.

In energy conversion, tungsten oxide nanoparticles are used as photocatalysts in water-splitting reactions, where they can use light to split water molecules into hydrogen and oxygen. This makes tungsten oxide nanoparticles an important material for the production of clean hydrogen fuel. Tungsten oxide nanoparticles can be synthesized through a variety of methods, including chemical synthesis and physical deposition [7]. They can also be engineered to improve their performance by changing their size, shape, or crystal structure.

Overall, tungsten oxide nanoparticles are a promising material in the fields of nanotechnology and energy due to their unique electronic and optical properties and their potential for use in gas sensing and energy conversion applications [8].

WO_3 nanoparticles are inorganic particles composed of tungsten and oxygen atoms. They are available in different morphologies such as nanorods, nanosheets, nanowires, or nanospheres. These nanoparticles have several interesting optical, electronic, and catalytic properties that make them useful in several fields. One of the significant applications of WO_3 nanoparticles is in gas and humidity sensing. WO_3 is efficient in detecting nitrous gas and also gives a rapid response to changes in environmental humidity. In addition, WO_3 nanoparticles can be used in electrochromic smart windows to minimize energy consumption by responding to light and temperature changes [9]. Furthermore, WO_3 nanoparticles have a high surface area and hence can provide an excellent catalyst for heterogeneous catalyst applications, especially in oxidation reactions. The nanoparticles are also used as a catalyst in photoelectrochemical (PEC) hydrogen evolution reactions in solar energy systems [10]. However, as with any nanoparticles, it is important to understand their potential toxicology and handling to ensure safe deployment in various industrial settings.

C. Liu et al. [11] in 2017, implementation of controls sol–gel dicarboxylic acid and polyethylene glycol were utilized as the chelating agent and polymeric source, respectively, in Pechini's approach to manufacturing WO_3 nanopowders. To create WO_3 powders, resin precursors were first calcined at 550°C with varying amounts of metal ions (12.5–50 mmol), acids (125–500 mmol), functionalization agents (32–262 mmol), and polyethylene glycol (1–16.5 mmol) in an environment of air. Energy dispersive spectroscopy, field emission scanning electron microscopy, and x-ray powder diffraction were used to analyze the materials. The findings showed that the WO_3 nanopowders aggregated in the monoclinic structure when made with various concentrations of chelating agent and polyethylene glycol. Because the polymerizing agent and polyethylene glycol were included in the inclusion of the polymerizing agent and polyethylene glycol as a source of carbon, the nanopowders were devoid of impurities. According to structural development, the concentration of polyethylene glycol and the complexing agent affected how the nanopowders changed from having a rod-like shape to being uniform and spherical. We obtained nanopowders with a confined size range and an average particle size of around 58 nm [11].

Jyothi Gupta et al. [12] in 2022, thin film technology has established itself in the fields of science and technology during the past 10 years. Certain purposes call for the improvement of various thin film characteristics. Porosity is one of the characteristics of thin films made of diverse materials that makes them particularly adaptable for use in a variety of applications. Porosity, which determines the volume of the hollow space over the entire span of the thin film, aids in improving and perfecting many thin-film-related application areas. One such area is electrochromic, where the porosity of thin films is crucial. One of the many useful and commonly used electrochromic materials, WO_3, is primarily used in implementations for electrochromic devices. Highly permeable WO_3 film can provide a significant improvement in a variety of applications, particularly in electrochromic devices. From this perspective, it becomes crucial to identify several strategies for improving the permeability of WO_3 thin films when using diverse deposition processes [12]. We have attempted to condense several physical vapor deposition (PVD) approaches in this article to improve the porosity of WO_3 thin films. Additionally, we have attempted to assess the impact of different process variables under various PVD procedures on the tailoring of the porosity of WO_3 thin films. Ultimately, we conclude by outlining several applications that include porous WO_3 thin films with technological advancement and are continually being improved.

W. Zhao et al. [13] in 2024 improve the photocatalytic overall water-splitting (POWS) process by addressing challenges in charge carrier separation and promotion. It focuses on both microscopic and macroscopic methods, including semiconductor catalyst optimization through energy band modulation to align with the water-splitting redox potential. The paper discusses various semiconductor materials, such as metal oxides, nitrides, sulfides, perovskites, carbon nitrides, and MOFs/COFs, and their role in enhancing POWS efficiency. Traditional semiconductor modification strategies like doping, heterojunction construction, and surface modification are analyzed for their impact on light absorption, charge dynamics, and charge output. The importance of electrostatic or polarization fields in these modifications is also emphasized. Furthermore, the paper explores the influence of external fields (electric, thermal, magnetic) on reaction systems and compares their effects on macroscopic carriers and reaction kinetics. Despite these efforts, challenges such as experimental time constraints, economic viability, instability due to natural light fluctuations, and inefficiency in large-scale systems remain. The paper concludes by discussing these issues and proposing strategies to address them moving forward.

2 | METHODOLOGY

A PVD Technique is used for the preparation of the WO_3 thin film because of its uniformity and purity; high uniformity, small area deposition with accuracy, and precise control over deposition conditions are essential. Indium tin oxide (ITO) has a higher transmittance in the visible and near-infrared regions, making it more suitable for applications requiring high optical transparency. ITO typically has a lower sheet resistance than FTO, which is beneficial for reducing energy losses and improving device performance. ITO has higher electrical conductivity due to its higher carrier concentration and mobility. ITO tends to have better adhesion to various materials, reducing the risk of delamination and improving device stability, and it is used in a broader range of applications, including displays, solar cells, and electrochromic devices, making it a more versatile material. It has a well-established manufacturing process, ensuring high quality and consistent material properties. ITO is more compatible with various materials and deposition techniques, making it easier to integrate into device fabrication processes.

2.1 | WO_3 thin film preparation

The first step to develop the thin film was to use thermal vapor deposition to deposit WO_3 on an ITO substrate. The starting material for the WO_3 thin film formation was 0.5 g of 99% pure WO_3 powder purchased from Sigma Aldrich. The tungsten boat was 99.9% pure WO_3. The tungsten-based boat and substrate holder (made of brass) were positioned 19 cm apart in the working chamber [14, 15]. A metal wrap contains a vacuum system, substance condensation, and vapor deposition on the substrate in this working chamber. Now, turn on the power supply and the Rotary Van Pump. Proper work can take up to 45 min. Turn on the water supply at the same time. The diffusion pump heater was then turned on to warm up the oil. Now, open the roughing valve until the pressure drops to 10^{-2} mbar. After closing the roughing valve, open the backup valve. Finally, connect the diffusion pump to the vacuum chamber by opening the isolation valve (Baffle Valve), achieving a vacuum of 10^{-5} mbar, turning on the transformer's power source, and applying a current of 75–85 A to electrically heat the tungsten boat containing WO_3 [16]. The source material was evaporated and deposited on the substrates using thermal energy. After deposition, close the baffle valve and turn off the diffusion pump, then let the rotary van pump and backing valve run for a while before closing the backing valve and shutting off the rotary van pump, turning off the main power, and allowing the water supply to run until the temperature of the flowing water returned to normal. On the Borosilicate and ITO substrates, a very thin film of WO_3 was deposited [17]. The thickness of the thin film was measured using a surface profilometer and found to be 65 nm.

3 | EXPERIMENTAL SECTION

Different characterization was done to explore the prepared thin film; X-rays diffraction (XRD) was done by using a D-8 Bruker x-rays diffractometer. Scanning electron microscopy (SEM) Cube-II (Tabletop SEM) Emcraft was used to investigate the surface morphology of the thin film, which has resolution imaging up to 2 nm and magnification of ×200,000. Fourier transform infrared (FTIR) setup Cary 630 Agilent Technologies, USA, ranging from 500 to 4500 wavelength (cm^{-1}) is used to identify the functional group, stretching, and expansion of the thin film. The absorbance and transmittance of the thin film were carried out to calculate the absorption of solar spectra of WO_3 thin film, while GC–MS, HPLC, Atomic Absorption Spectrophotometer, and Gemmary Galvano-potentio state CV setup were used for impedance, linear sweep voltammetry (LSV), and hydrogen evolution during the water splitting of the thin film.

4 | RESULT AND DISCUSSION

4.1 | XRD study

The XRD analysis of nanoparticles is a common technique used to study the crystal structure and phase identification of nanoscale materials. XRD is particularly useful in characterizing nanoparticles because it can provide information about their crystallographic properties, such as crystal size, lattice parameters, and preferred orientation [18]. The XRD peaks (101) (103) (004) (200), (105) (211) (116), (220) in Figure 1 depict the spectra of WO_3 thin films grown on an ITO substrate by PVD technique, while the asterisk peak shows the ITO peaks in the XRD study. The WO_3 XRD investigation demonstrates the synthesis of an orthorhombic structure (JCPDS Card no. 35–0270), pointing to the development of single-phase and polycrystalline WO_3 thin films, without any sign of secondary phases [19]. Figure 1 demonstrates that the major reflection, which is particularly intense and denotes a preferred orientation in the deposited WO_3 thin film, is located in the positions of the reflection planes of the WO_3 film at $2\theta = 23.14°$, 23.70°, and 24.36°. The calculated crystallite size, 16.43 nm, according to the Debye–Scherrer formula [20] indicates a comparatively small size that increases grain boundaries and makes it appropriate for hydrogen generation applications.

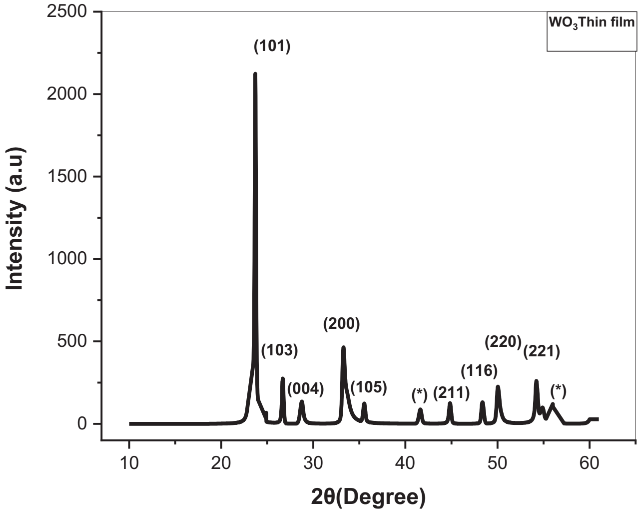

FIGURE 1 XRD analysis of WO_3.

$$D = \frac{k \times \lambda}{\beta \mathrm{Cos}\theta}. \qquad (1)$$

4.2 | SEM study

SEM scans of ITO usually show a polycrystalline structure with discernible grains that vary in size from 34 nm to a few micrometers. At greater magnifications, the normally smooth surface may exhibit microporosity or a little roughness, which can affect characteristics like electrical conductivity and optical transparency. The grain boundaries shown in SEM images of ITO films, which are usually deposited on glass or flexible substrates, are essential for conductivity and adhesion in applications such as transparent electrodes, solar cells, and displays. The performance of the ITO film can be enhanced by post-deposition annealing or other treatments that improve the grain structure, as reported in Figure 2.

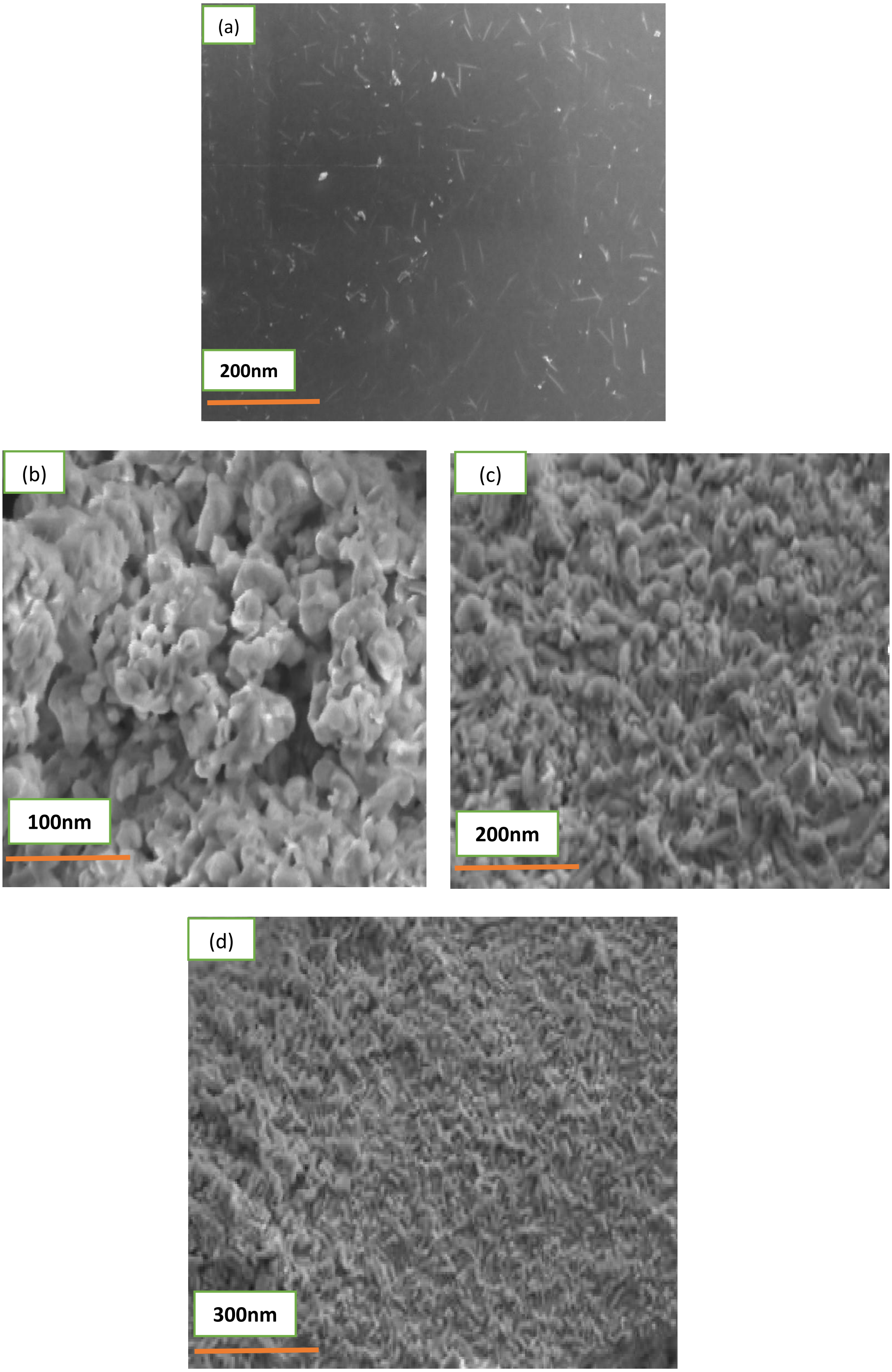

FIGURE 2 (a) SEM Analysis of ITO substrate. (b–d) SEM analysis of WO_3 thin film at various resolutions.

WO_3 thin films prepared via PVD, SEM images often show a dense, smooth surface with relatively uniform coverage, though variations can appear depending on specific parameters. At higher magnifications, SEM can reveal well-defined grains, with sizes ranging from tens to hundreds of nanometers, or even larger, depending on the film's thickness and growth conditions [21]. Moreover, the thin films appear featureless, further emphasizing their consistent and uniform nature.

The observed outcome, extremely low roughness of the WO_3 thin films, can be attributed to surface adatom mobility, which is critical in preventing the formation of voided columnar microstructures. Surface adatom mobility refers to the movement of atoms or molecules on the surface of a material [22]. About WO_3 thin films, the presence of mobile adatoms during the deposition process facilitates the formation of a smooth and uniform surface by reducing the chances of voids or irregularities. This phenomenon helps to inhibit the growth of columnar structures that are typically associated with rough surfaces and nonuniform coatings. The overall smooth and uniform morphology of the WO_3 thin films is highly desirable for hydrogen production [23].

The SEM study of WO_3 in Figure 2b–d at different resolutions was recorded and observed; when the scan rate increases, the visibility of the morphology increases due to slower scan rates providing more time for the electron beam to interact with the sample surface, which improves resolution, enhances signal detection, and allows finer details like grain size to be visible. Faster scan rates limit these interactions, leading to lower resolution and less visibility of small features. The grain size of WO_3 was measured to be 34 nm, which is quite better for water splitting.

Changing the resolution scan rate of an SEM impacts thin film imaging. A higher scan rate (faster scan) provides lower resolution, faster scanning, and less detail, while a lower scan rate (slower scan) offers higher resolution but may cause surface heating or artifacts. The optimal scan rate balances the need for detail with the sensitivity of the thin film to electron beam exposure.

The scan rate can affect the thin film's physical, chemical, and functional properties by influencing factors like surface temperature, structural integrity, and material composition. A balance must be found to avoid compromising the film's performance while obtaining the desired resolution in SEM imaging [24].

4.3 | Brunauer–Emmett–Teller analysis

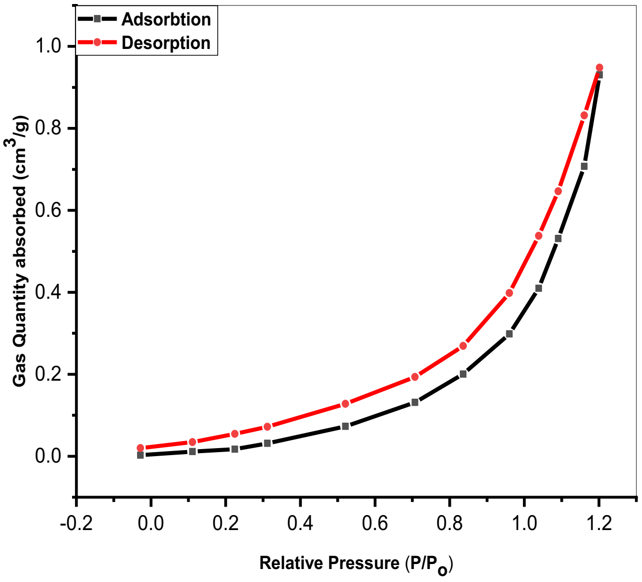

FIGURE 3 Surface analysis of the WO_3 thin film using the BET method.

The Brunauer–Emmett–Teller (BET) analysis is mostly used to calculate surface area and porosity in materials, particularly in thin films. It is based on the physical adsorption of gas molecules (typically nitrogen) onto the material's surface and is primarily used to determine surface area, pore size, and pore volume, all of which are critical for understanding the material's performance in a variety of applications, including catalysis, sensors, and energy storage devices.

The BET (a Micromeritics Tristar 3000) study was used to investigate the porous surface of the WO_3 thin film and the surface analysis. Figure 3 shows a traditional IV sorption isotherm accompanied by an H1-type hysteresis loop in the N_2 adsorption–desorption isotherms of a WO_3 thin film. It clearly demonstrates that capillary condensation is connected with large pore channels in WO_3 pyramidal formations. The BET analysis shows that the WO_3 thin film has a surface area of $73.74\ m^2\ g^{-1}$. The WO_3 thin film has a wide surface area and mesopores, potentially accelerating the reaction due to the high number of active sites. Such a large surface area material is useful for photocatalytic activity, which provides extra active surface sites for the adsorption of organic compounds, which enhances the photocatalytic efficiency. The adsorption isotherms of the layered WO_3 thin film exhibit hysteresis loops, which are the main characteristics of the porous structure. It is used to calculate the actual surface area available for the surface reactions (oxidation and reduction) [25–27].

BET study of WO_3 thin films reveals surface area, pore structure, and overall qualities that impact performance in applications such as catalysis and energy storage. The analysis is vital for adapting the material's properties to specific applications.

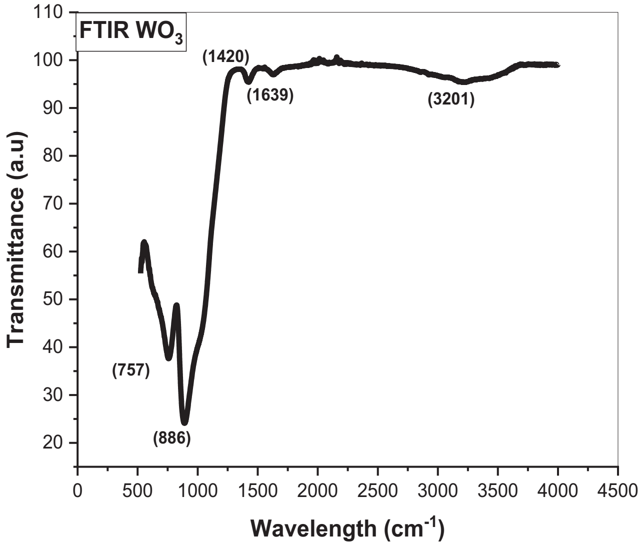

FIGURE 4 FTIR analysis of WO_3 thin film.

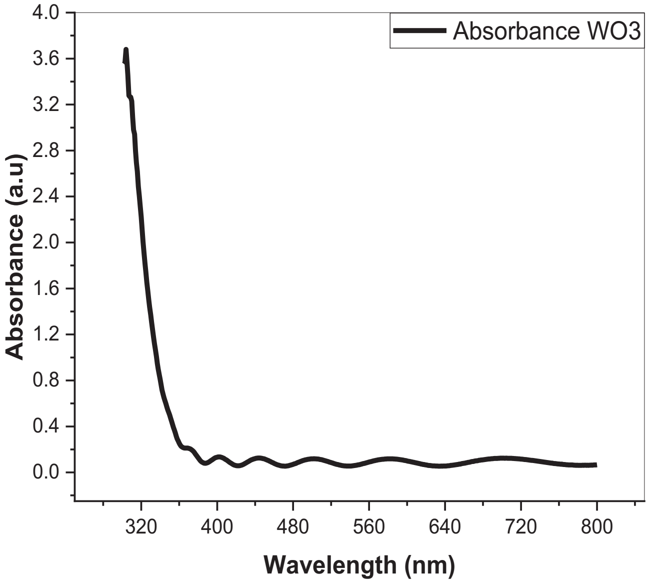

FIGURE 5 UV-vis spectroscopy of WO_3 thin film.

4.4 | FTIR analysis

FTIR spectroscopy was used to investigate the chemical bonding states, intricate structure, and functional groups of the synthesized WO_3 thin films [28]. With KBr as the medium, FTIR spectra in the 4500–400 cm^{-1} wavenumber range were captured. This study focused on the spectral region between 547 and 678 cm^{-1}. The stretching vibration of a surface hydroxyl group causes the band seen at 3201 cm^{-1}, which is most likely a sign of re-adsorption of water from the surrounding atmosphere. On the other hand, the tungsten-hydroxyl (W-OH) bond's stretching vibration is linked to the band at 1639 and 1420 cm^{-1}. In Figure 4, distinctive strong absorptions were observed at approximately 757 and 886 cm^{-1}, which can be attributed to the W=O and O-W-O stretching vibrations, respectively, arising from the formation of crystalline WO_3 [29]. Notably, these specific absorptions were only observed in the crystalline WO_3 film and were not present in the amorphous WO_3 film. Minor peaks are observed in the range of 1400–1700 cm^{-1} due to bending vibrations of the hydroxyl group (δ(O-H)) and water absorption bands, which are present due to the humidity in the environment or residual water during the film preparation process as reported in Figure 4.

4.5 | UV-vis spectroscopy

To investigate the optical characteristics of semiconducting materials, useful techniques like UV-visible diffuse reflectance and absorbance spectroscopy are frequently employed. As shown in Figure 5, absorbance spectra of the WO_3 thin film were examined at various WO_3 content levels and wavelengths ranging from 300 to 800 nm.

One notable observation is that the WO_3 thin film demonstrates higher reflectance than other metal oxides [30]. However, this reflectance decreases as the wavelength increases [27, 28]. This reduction in reflectance can be attributed to the enhancement of lattice defects in the thin film, which subsequently leads to increased absorption.

Regarding the UV-visible optical absorption spectra of the WO_3 samples, they exhibit relatively high absorbance beyond 400 nm due to their band gap energy and optical properties, which limit the absorption of photons with wavelengths longer than those in the visible blue-violet region, as reported in Figure 5. WO_3 has a wide band gap, typically around 2.5 to 3.5 eV, which means it absorbs light in the UV region and is often used in photocatalysis for applications such as water splitting and environmental cleanup under UV light. Interestingly, the results indicate a wavelength fluctuation around 385 nm, which may be attributed to inter-band charged transitions involving trapping electrons [31, 32]. WO_3 is generally less absorptive in the near-infrared region unless modified. For some infrared applications, doping can enhance absorbance in the NIR range.

4.6 | Transmittance analysis

The transmittance of WO_3 indicates that the thin film possesses high transparency, with a transparency value of 88.67% in the visible region due to WO_3 thin films being

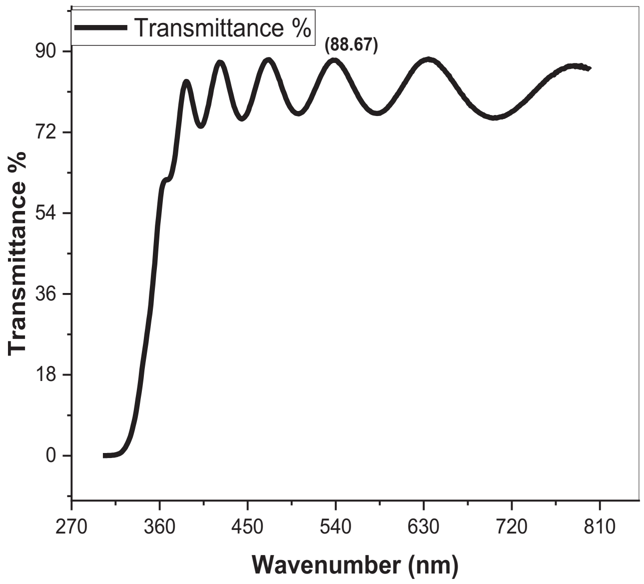

FIGURE 6 Transmittance of WO_3 thin film.

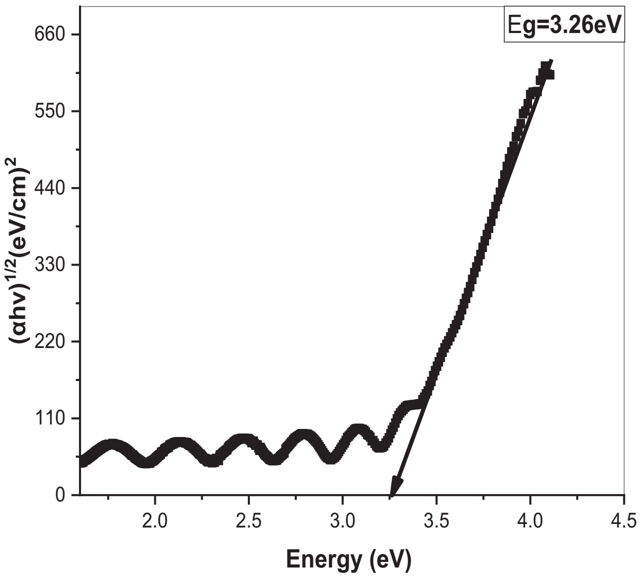

FIGURE 7 Tauc's plot of WO_3 thin film.

transparent in the visible range due to their wide band gap, low visible light absorption, controlled film thickness, and specific microstructural properties, all of which enable high visible light transmittance, as cited in Figure 6. This high level of transparency suggests that the film exhibits excellent optical quality, and it also indicates minimal absorption losses [33].

Furthermore, the presence of fringes at higher wavelengths serves as confirmation that the WO_3 thin film was successfully prepared without any inhomogeneity. The absence of inhomogeneity is a positive sign of the film's uniformity and overall structural integrity [34].

4.7 | Band gap determination

The well-known Tauc's relationship was also used to calculate the bandgap energy of the WO_3 thin films as reported in Figure 7. The following expression was used to analyze the optical absorption edge:

$$\alpha = 1/d \ln\left(1/T\right). \tag{2}$$

In this equation, d represents film thickness, while T denotes transmittance. The absorption coefficient (α) depends on the photon energy absorbed strongly by the thin films. To measure the bandgap of the metal oxide semiconductors, the widely used Tauc relation is applied:

$$(\alpha h v) = \beta(h\nu - \mathrm{Eg})^{\eta}. \tag{3}$$

The absorption coefficient α, Planck's constant h, photon frequency (ν), incident photon energy ($h\nu$), and optical bandgap energy are all represented in this context by the letters α, h, ν, h, and Eg, respectively [35]. The variables β and η depend on the likelihood of a transition occurring and its direction, which can be either direct or indirect. In Figure 7, the plot displays an indirect transition as $(\alpha h)^{1/2}$ with $h\nu$ changes linearly [36].

By extrapolating the $(\alpha h\nu)^{1/2}$ versus energy ($h\nu$) curve, the estimated bandgap value of pure WO_3 thin film was found to be 3.26 eV, which is essential for applications in photocatalysis.

4.8 | Electrochemical impedance spectroscopy study

Electrochemical Impedance Spectroscopy (EIS) measurements were conducted in the dark using an Autolab PGSTAT-30 potentiostat with a frequency analyzer. To ensure the stability of the WO_3 film, an AC signal of 20 mV was applied across a frequency range of 50 Hz to 10 kHz within a restricted potential window at a constant bias voltage. EIS was performed to gain insight into the reaction kinetics of the system [37, 38].

The charge transfer properties of different counter electrodes at the electrode/electrolyte interface, EIS analysis was conducted on symmetric cells containing two identical electrodes [39]. For the EIS experiments, a symmetric cell was fabricated using WO_3 as the working electrode and Platinum as the counter electrode (CE). The EIS analysis revealed semicircles in the Nyquist plots, representing the charge transfer processes at both the CE/electrolyte interface and the electrolyte interface, respectively, as recorded in Figure 8. The low impedance

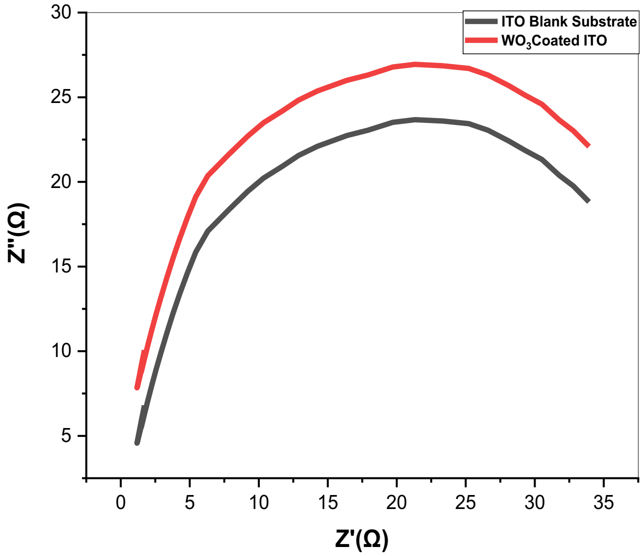

FIGURE 8 EIS plot of WO_3.

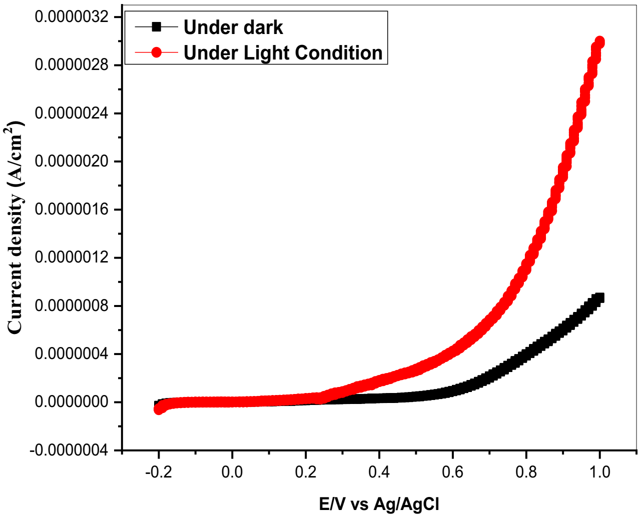

FIGURE 9 LSV measurements of WO_3 thin film.

curve observed for the WO_3-based cell indicates efficient charge transfer from the electrolyte interface to the working electrode [40]. This suggests that WO_3 demonstrates excellent charge transfer characteristics, leading to maximum photocurrent generation under suitable wavelengths within the solar spectra.

In the Nyquist plot, the presence of a semicircle indicates charge transfer resistance, which provides information on the rate of electron transfer within the material. The diameter of this semicircle reflects the reaction kinetics, with a larger diameter typically indicating slower charge transfer [41].

4.9 | LSV measurements

Linear sweep voltammetry measurements were conducted in the dark using an Autolab PGSTAT-30 potentiostat with a frequency analyzer. To ensure the stability of the WO_3 film, an AC signal of 20-mV amplitude was applied across a frequency range of 50 Hz–10 kHz within a controlled potential range and at a fixed bias voltage.

LSV is a technique used to study the process of water splitting into hydrogen and oxygen by applying an increasing voltage. Initially, no voltage is applied, so no reaction occurs. As the voltage is gradually increased, water begins to break down into hydrogen (H_2) and oxygen (O_2) gases. During this process, the flow of electrons also increases, causing the current to rise. This rise in current indicates how easily water splits at different voltages. At a certain voltage, the water splits more rapidly, and the current increases more quickly, signaling that the process is becoming more efficient. Overall, LSV helps researchers determine the voltage required to split water and measure the efficiency of hydrogen and oxygen production.

The prepared WO_3 thin film's solar light hydrogen conversion efficiency (STH%) was calculated using the formula below:

$$\text{STH\%} = \frac{(1.23 - V_{\text{bias}})J}{P} \times 100\%, \tag{4}$$

where V_{bias} represents the applied voltage using solar spectra between the working and reference electrodes (AgCl/Ag). J denotes the photocurrent density generated by the WO_3 thin film [42]. P is the solar intensity at the Earth's surface, which is typically 100 mW/cm^2.

Upon experimental measurement, the STH% of the WO_3 thin film was found to be 0.51% at an applied voltage of 0.8 V.

To further understand the change in photocurrent under different conditions, the following formula was utilized:

$$J = J_{\text{light}} - J_{\text{dark}}. \tag{5}$$

In this context:

J_{light} represents the photocurrent density measured under light conditions.

J_{dark} represents the photocurrent density measured under dark conditions (i.e., in the absence of light).

The difference between the photocurrent under light and dark conditions, as reported in Figure 9, gains insights into the light-induced changes in photocurrent due to the presence of the WO_3 thin film. This suggested that WO_3 yields a significantly higher current at a higher wavelength [42–46].

The difference between the photocurrent under light and dark conditions reported in Figure 9, gains insights into the light-induced changes in photocurrent due to the presence of the WO_3 thin film. This suggested that WO_3 yields a significantly higher current at a higher wavelength [45, 47].

4.10 | Hydrogen generation measurement

Photoelectrochemical water splitting is a promising method for producing hydrogen, with its effectiveness heavily reliant on the light source used. The UV-visible wavelength range commonly used spans 200 to 500 nm, with light intensities from 10 to 100 mW/cm^2 and irradiance levels between 100 and 1000 W/m^2. Typical light sources in PEC water-splitting research include xenon lamps, LED arrays (such as UV, blue, or white LEDs), solar simulators, and lasers at specific wavelengths [48].

4.10.1 | Water-splitting mechanism

The hydrogen generation process in water splitting breaks down water into hydrogen and oxygen gases using electricity. This happens in two steps. First, at the anode (positive side), water molecules are split, releasing oxygen gas, protons (hydrogen ions), and electrons. The reaction at the anode is

$$2H_2O \rightarrow O_2 + 4H^+ + 4e^-.$$

The released electrons travel through an external circuit to the cathode (negative side), where they combine with protons to form hydrogen gas. The reaction at the cathode is

$$4H^+ + 4e^- \rightarrow 2H_2.$$

The overall reaction is the splitting of water into hydrogen and oxygen gases

$$2H_2O \rightarrow 2H_2 + O_2.$$

The efficiency of this process depends on the voltage applied, the use of catalysts, and the system setup. The minimum voltage required for this to happen is 1.23 V, but higher voltages are often needed in practice due to losses. Catalysts like iridium or platinum are used to make the process more efficient by lowering the energy required for the reactions to occur.

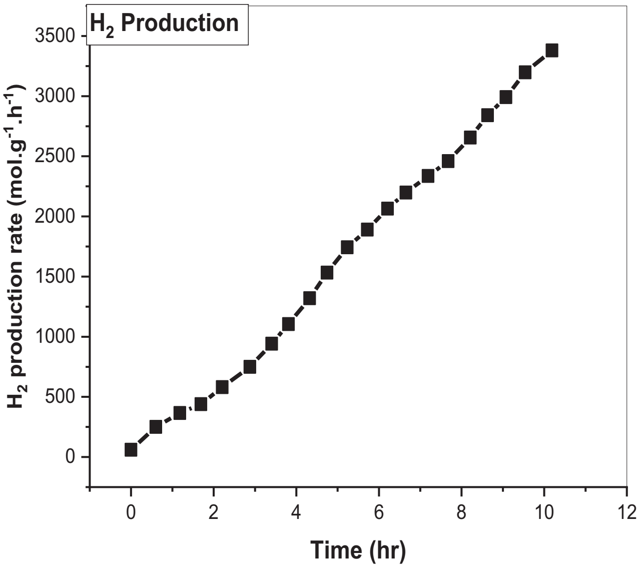

FIGURE 10 Hydrogen production rate versus time.

WO_3 is a n-type semiconductor with an indirect band gap in its most stable orthorhombic phase, with a value around 3 to 3.5 eV. This indirect band gap structure generally results in lower absorption efficiency compared to direct band gap materials, especially in the visible light range. The rate at which the WO_3 thin film produces hydrogen is reported in Figure 10. It was discovered that WO_3 produces hydrogen at a higher rate than other metal oxide materials [49]. The exceptional solar light harvesting abilities of the thin film, which have been demonstrated by numerous tests like absorbance, electrochemical impedance spectroscopy, and LSV, are responsible for the increased hydrogen production rate [46–50]. The remarkable hydrogen production rate is significantly influenced by the WO_3 thin film's porosity, which was discovered through analysis using scanning electron microscopy. The presence of porosity facilitates efficient hydrogen evolution reactions, thereby contributing to the overall increase in the hydrogen generation rate. To provide more detail about the hydrogen production rate of WO_3 [51–54].

It was found to have an average hydrogen production rate of 1743.09 mol g^{-1} in 6 h reported in Figure 10. This significant rate highlights the potential of WO_3 as a promising candidate for hydrogen evolution and renewable energy applications as compared to the other metal oxides cited in the literature.

5 | CONCLUSIONS

In summary, WO_3 thin films exhibit highly promising features for PEC water splitting, primarily due to their remarkable light absorption and efficient charge transfer properties. XRD analysis revealed the formation of an orthorhombic crystal structure with a crystallite size of 16.43 nm, which enhances the grain boundaries, contributing to better performance in hydrogen generation. SEM and FTIR spectroscopy indicated that the WO_3 films possess a smooth, uniform surface with minimal roughness, which is ideal for photocatalytic applications. UV-vis analysis demonstrated that the films are highly transparent, with substantial light absorption in the visible range, which is essential for effective photocatalysis. The band gap of WO_3, calculated to be 3.26 eV using Tauc's plot, confirms its ability to absorb light in the visible spectrum, making it suitable for photocatalytic applications. EIS and LSV measurements showed that the WO_3 films exhibit efficient charge transfer properties and generate high photocurrents under illumination, further enhancing their potential in PEC water splitting. The hydrogen production rate measured for WO_3 was 1743.09 mol g^{-1} h^{-1}, which is notably higher than that of many other materials, underscoring its superior performance in hydrogen evolution. The overall combination of high light absorption, efficient charge transfer, and a high hydrogen production rate makes WO_3 a highly promising material for renewable energy applications, particularly in the field of solar-driven hydrogen generation.

ACKNOWLEDGMENTS

The authors extend their appreciation to King Saud University, Saudi Arabia, for funding this work through Researchers Supporting Project number (RSPD2025R704), King Saud University, Riyadh, Saudi Arabia.

CONFLICT OF INTEREST STATEMENT

The authors declare no conflicts of interest.

DATA AVAILABILITY STATEMENT

The data that support the findings of this study are available from the corresponding author upon reasonable request.

ORCID

Muhammad Junaid https://orcid.org/0000-0001-8641-2185

REFERENCES

[1] H. Wu, J. Li, L. Tian, F. Zhao, J. Yin, Y. Shao, *Chem. Eng. J.* **2024**, *495*, 153608.
[2] J. Wei, P. Fan, Y. Huang, H. Zeng, R. Jiang, Z. Wu, Y. Zhang, Z. Hu, *Org. Chem. Front.* **2024**, *12*, 3459. https://doi.org/10.1039/D4QO00444B
[3] L. Wang, H. Hu, C.-C. Ko, *J. Funct. Biomater.* **2024**, *15*, 211.
[4] C. Feng, Y. Shi, J. Hao, Z. Wang, Z. Mao, G. Li, Z. Jiang, *Petrol. Explor. Dev.* **2017**, *44*, 274.
[5] Y. Yao, S. Chen, *Biotechnol. Biofuels* **2016**, *9*, 115.
[6] X. Hou, L. Qiu, S. Luo, K. Kang, M. Zhu, Y. Yao, *RSC Adv.* **2018**, *8*, 40941.
[7] L. Qiu, Y. F. Deng, F. Wang, M. Davaritouchaee, Y. Q. Yao, *Renew. Sustain. Energy Rev.* **2019**, *115*, 109373.
[8] H. Wu, A. Li, H. Zhang, S. Li, C. Yang, H. Lv, Y. Yao, *Microbiome* **2024**, *12*, 170.
[9] D. Wang, J. Ou-Yang, W. Guo, X. Yang, B. Zhu, *Ceram. Int.* **2017**, *43*, 9573.
[10] L.-C. Zhao, Y. Liu, Z. Wang, N. Tang, J. Leng, B. Zheng, Y.-Y. Liu, W. Li, *Int. J. Pharmacol.* **2018**, *14*, 952.
[11] C. Liu, Z. Li, H. Zhang, H. Yu, J. Yan, D. Wei, Z. Song, J. Cao, Y. Sun, *Anal. Chim. Acta* **2023**, *1279*, 341779.
[12] B. Zhu, Z. Wang, Y. Zhang, Z. Yu, J. Shi, R. Xiong, *Mater. Chem. Phys.* **2009**, *113*, 746.
[13] X. Ji, P. Jiang, Y. Jiang, H. Chen, W. Wang, W. Zhong, X. Zhang, W. Zhao, D. Zang, *Adv. Sci.* **2023**, *10*, 2300049.
[14] H. Zhou, J. Guo, G. Zhu, H. Xu, X. Tang, X. Luo, *Sep. Purif. Technol.* **2024**, *334*, 126086.
[15] Y. Wang, S. Xia, K. Chen, J. Zhang, H. Tan, C. Yu, J. Cui, J. Zeng, J. Wu, P. Wang, Y. Wu, *ACS Nano* **2024**, *18*, 34403.
[16] B. Zhuang, Y. Yang, K. Huang, J. Yin, *Opt. Lett.* **2024**, *49*, 6489.
[17] Z. Hua, H. Song, C. Zhou, Q. Xin, F. Zhou, W. Fan, S. Liu, X. Zhang, C. Zheng, Y. Yang, X. Gao, *Chem. Eng. J.* **2023**, *473*, 145106.
[18] G. Wang, W. Feng, *Opt. Express* **2023**, *31*, 39500.
[19] Y. Xie, J. Dong, Y. Li, X. Ma, N. Wang, X. Meng, Y. Huang, *Acta Mater.* **2025**, *286*, 120706.
[20] J. Zheng, C. Weng, C. Tian, W. Zhang, J. Qin, X. Li, W. Liu, J. Zhang, Z. Lin, *Chem. Eng. J.* **2024**, *491*, 152122.
[21] H. Zhao, T. Zhang, S. Chen, G. Zhao, *Nano Lett.* **2025**, *25*, 2647. https://doi.org/10.1021/acs.nanolett.4c05232
[22] C. Han, H. Wang, Z. Wang, X. Ou, Y. Tang, *Adv. Mater.* **2023**, *35*, 2300917. https://doi.org/10.1002/adma.202300917
[23] Y. Wei, B. Tang, X. Liang, F. Zhang, Y. Tang, *Adv. Mater.* **2023**, *35*, 2302086. https://doi.org/10.1002/adma.202302086
[24] Q. Wan, R. Liu, Z. Zhang, X. Wu, Z. Hou, L. Wang, *Chin. J. Chem.* **2024**, *42*, 1913. https://doi.org/10.1002/cjoc.202400058
[25] X. Xu, X. Feng, W. Wang, K. Song, D. Ma, Y. Zhou, J. Shi, *J. Colloid Interface Sci.* **2023**, *651*, 669.
[26] C. Wang, C. Feng, M. Wang, X. Li, P. Cheng, H. Zhang, Y. Sun, P. Sun, G. Lu, *RSC Adv.* **2015**, *5*, 29698.
[27] W. Zeng, B. Miao, T. Li, H. Zhang, S. Hussain, Y. Li, W. Yu, *Thin Solid Films* **2015**, *584*, 294.
[28] D. Wei, M. J. Bailey, P. Andrew, T. Ryhänen, *Lab Chip* **2009**, *9*, 2123.
[29] D. Chen, Y. Li, X. Li, X. Hong, X. Fan, T. Savidge, *Chem. Sci.* **2022**, *13*, 8193.
[30] F.-Z. Yao, Q. Yuan, Q. Wang, H. Wang, *Nanoscale* **2020**, *12*, 17165.
[31] S. Cong, F. Geng, Z. Zhao, *Adv. Mater.* **2016**, *28*, 10518.
[32] G. Yang, X. Zhu, G. Cheng, R. Chen, J. Xiong, W. Li, Y. Wei, *J. Mater. Chem. A* **2021**, *9*, 22781.
[33] Z. Hai, Z. Wei, C. Xue, H. Xu, F. Verpoort, *J. Mater. Chem. C* **2019**, *7*, 12968.
[34] W. Zhao, H. Chen, J. Zhang, P. J. Low, H. Sun, *Chem. Sci.* **2024**, *15*, 17292.

[35] L. Huang, Y. Zhao, D. Cai, *Mater. Lett.* **2009**, *63*, 2082.

[36] X. Yi, L. Wang, K. Mochizuki, X. Zhao, *J. Phys. D: Appl. Phys.* **1988**, *12*, 1755.

[37] A. Rios-Flores, O. Arés, J. M. Camacho, V. Rejon, J. L. Peña, *Solar Energy* **2012**, *86*, 780.

[38] J. H. Kwon, J. Park, M. K. Lee, J. W. Park, Y. Jeon, J. B. Shin, M. Nam, C. K. Kim, Y. K. Choi, K. C. Choi, *ACS Appl. Mater. Interfaces* **2018**, *10*, 15829.

[39] S. A. Adewinbi, R. A. Busari, O. E. Adewumi, B. A. Taleatu, *Surf. Interfaces* **2021**, *23*, 101029.

[40] J. H. Kwon, S. Choi, Y. Jeon, H. Kim, K. S. Chang, K. C. Choi, *ACS Appl. Mater. Interfaces* **2017**, *9*, 27062.

[41] T. Wang, Y. Guo, P. Wan, H. Zhang, X. Chen, X. Sun, *Small* **2016**, *12*, 3748.

[42] L. A. Nafie, N. S. Lee, G. Paterlini, T. B. Freedman, *Microchim. Acta* **1987**, *93*, 93.

[43] Y. C. Cha, C. E. Kim, S. Lee, H. J. Hwang, J. W. Moon, S. Han, S.-K. Woo, *Synthesis of silica aerogel thin film from waterglass*. **2007**.

[44] Z. Lian, H. Li, T. Wu, J. Zhao, S. Cai, R. Yang, *Appl. Surf. Sci.* **2022**, *606*, 154874.

[45] B. Han, M. Gao, Y. Wan, Y. Li, W. Song, Z. Ma, *Mater. Sci. Semicond. Process.* **2018**, *75*, 166.

[46] Q. T. Vu, *Electrophoretic deposition of semiconducting polymer metal oxide nanocomposites and characterization of the resulting films*. **2006**.

[47] Y. Kim, W. J. Woo, D. Kim, S. Lee, S. M. Chung, J. Park, H. Kim, *Adv. Mater.* **2021**, *33*, 2005907.

[48] Y. Wang, *One Dimensional Hierarchical Nanomaterials Derived from M-MoO4 (M= Ni, Co) as Highly Effective Electrocatalysts for Water Splitting*, Monash University, Melbourne, Victoria, **2019**.

[49] J. Singh, G. Kaur, M. Rawat, *J. Bioelectron. Nanotechnol* **2016**, *1*, 9.

[50] Y. Abboud, T. Saffaj, A. Chagraoui, A. El Bouari, K. Brouzi, O. Tanane, B. Ihssane, *Appl. Nanosci.* **2014**, *4*, 571.

[51] B. D. Keller, *Emerging Electronic Materials: Thin Films of Asphaltenes and Coal Nanoparticles for Electronic Devices and Large Area Layer Controlled 2-Dimensional Semiconductor Synthesis*, Massachusetts Institute of Technology, Cambridge, MA, **2016**.

[52] M. Junaid, K. M. Batoo, S. G. Hussain, W. Q. Khan, S. Hussain, *Results Chem.* **2023**, *6*, 101102.

[53] M. Junaid, *Luminescence* **2024**, *39*, e70020. https://doi.org/10.1002/bio.70020

[54] M. Junaid, K. M. Batoo, M. F. Ijaz, B. Zazoum, *Luminescence* **2024**, *39*, e4821.

How to cite this article: M. Junaid, M. Sharaf, M. El-Meligy, M. A. Riaz, M. A. Dar, I. U. Khan, *J. Chin. Chem. Soc.* **2025**, 1. https://doi.org/10.1002/jccs.202500009